Chemical Science

ROYAL SOCIETY OF CHEMISTRY

EDGE ARTICLE

View Article Online
View Journal | View Issue

Cite this: *Chem. Sci.*, 2024, **15**, 11435

All publication charges for this article have been paid for by the Royal Society of Chemistry

Received 2nd May 2024
Accepted 18th June 2024

DOI: 10.1039/d4sc02899f

rsc.li/chemical-science

A multi-resonance emitter with five-membered thiophene as the π-core enables efficient, narrowband and reduced efficiency roll-off OLEDs†

Linjie Li,[a] Jiaqi Li,[c] Lixiao Guo,[a] Yincai Xu,[a] Yifan Bi,[a] Yexuan Pu,[a] Pingping Zheng,[a] Xian-Kai Chen,*[c] Yue Wang[ad] and Chenglong Li*[ab]

Efficient, narrowband multi-resonance thermally activated delayed fluorescence (MR-TADF) emitters have recently sparked significant interest in high-resolution organic light-emitting diode (OLED) displays. However, almost all the progress in MR-TADF materials has been accomplished using a six-membered ring as the π-core to date. Herein, we present the first example of a five-membered ring π-core-based MR-TADF emitter named Th-BN developed by introducing thiophene instead of hexagonal benzene as the π-core. The introduction of thiophene significantly enhances intramolecular charge transfer intensity and the spin–orbit coupling matrix elements but does not change the intrinsic MR properties. As a result, Th-BN exhibits a narrowband green emission at 512 nm, with a high luminous efficiency of 97%, a narrow full-width at half maximum of 41 nm/0.20 eV, and a rapid reverse intersystem crossing rate of 18.7×10^4 s^{-1}, which is 10 times higher than that of its benzenoid counterpart DtBuCzB. The corresponding green OLEDs based on Th-BN achieve excellent electroluminescence performance with an external quantum efficiency (EQE) of 34.6% and a reduced efficiency roll-off with an EQE of 26.8% at a high luminance of 1000 cd m^{-2}.

Introduction

Organic light-emitting diodes (OLEDs) with narrowband emission are of great significance in the development of energy-saving and high color purity displays due to a larger color gamut space compared to conventional liquid crystal displays.[1–3] In general, for the latest commercial OLED displays, narrow electroluminescence (EL) spectra can be obtained by using color filters or optical microcavities.[4–6] However, this can lead to significant energy loss and increased manufacturing cost.[7,8] In 2016, Hatakeyama and coworkers developed a new paradigm termed multi-resonance induced thermally activated delayed fluorescence (MR-TADF) based on boron- and nitrogen-embedded polycyclic aromatics.[9] The opposite resonance effect of boron and nitrogen atoms induces the localization of the highest occupied and lowest unoccupied molecular orbitals (HOMO and LUMO) on different atoms and minimizes their bonding/antibonding character.[10–15] Benefiting from the rigid polycyclic skeleton and multi-resonance effect, these MR-TADF materials exhibit not only extremely high photoluminescence quantum yields (PLQY) and TADF activity but also small full-width at half maximum (FWHM) due to the suppressed vibronic coupling between the ground state (S_0) and the lowest energy singlet excited state (S_1), as well as the structural relaxation of the S_1 state.[16–18] In the last few years, tremendous progress has been made in developing MR-TADF emitters with high efficiency and high color purity for blue,[19–25] green[26–31] and red[32–38] OLEDs. However, a crucial drawback of the current MR-TADF system is the rather slow reverse intersystem crossing (RISC) process derived from long delay lifetimes of several tens of microseconds, which leads to severe efficiency roll-off at high brightness. In addition, to the best of our knowledge, almost all the developed MR-TADF emitters exclusively consist of benzenoid rings as a central π-core, limiting the structural diversity of the MR-TADF molecular library (Fig. 1a). Very recently, we have developed a series of non-benzenoid π-core-based MR-TADF (NB-MR-TADF) emitters for the first time, utilizing pyridinyl or pyrimidine as the π-core.[39] These compounds exhibited ultra-narrowband deep-blue emissions with peaks at 440 and 409 nm and FWHMs of 14 and 13 nm. Almost immediately, Zhang and co-workers synthesized a MR-TADF molecule centered on a pyridine ring, showing a bright orange-red emission peaking at 586 nm with a FWHM of 40 nm.[40] These

[a]State Key Laboratory of Supramolecular Structure and Materials, College of Chemistry, Jilin University, Changchun 130012, P. R. China. E-mail: chenglongli@jlu.edu.cn

[b]Chongqing Research Institute, Jilin University, Chongqing 401120, P. R. China

[c]Institute of Functional Nano and Soft Materials (FUNSOM), Soochow University, Suzhou 215123, P. R. China

[d]Jihua Laboratory, 28 Huandao South Road, Foshan 528200, Guangdong Province, P. R. China

† Electronic supplementary information (ESI) available: Compound syntheses and characterization, other theoretical calculations, spectra and other device performances. See DOI: https://doi.org/10.1039/d4sc02899f

results demonstrate the great potential of NB-MR-TADF emitters for constructing high-performance narrowband emitters and OLEDs.

Thiophene is a well-known, electron-rich, five-membered non-benzenoid aromatic hydrocarbon that contains sulfur (S) as a heteroatom.[41–44] It has gained popularity as a building block for organic solar cells[45–48] and materials[49–52] arising from a combination of its stability, efficient π-conjugation, and versatile functionalization chemistry. Nevertheless, no example of thiophene π-core-based MR-TADF emitters has been reported, and their advantages compared with their six-membered aromatic ring counterparts in optoelectronic devices have not been revealed. In this contribution, we report for the first time five-membered ring π-core-based MR-TADF emitter Th-BN (Fig. 1b), in which the benzene ring is replaced with thiophene as the π-core. For comparison, we selected the simple and classical carbazole-embedded MR-TADF molecule DtBuCzB with a benzene ring as the π-core (Fig. 1a).[53] Compared to the benzene ring, the introduction of a thiophene π-core in the MR-TADF backbone can break the symmetry of the molecular structure and alter the spatial distributions of the frontier molecular orbitals (FMOs) of the central π-core, resulting in a significantly increased intramolecular charge transfer intensity. Consequently, a red shift of the emission peak can be expected. In addition, the introduction of a S (SN = 16) atom in thiophene can enhance not only the heavy-atom effect, but also the nπ* character of the S_1 state, promoting the spin–orbit coupling (SOC) matrix elements between singlet and triplet excited states, which is advantageous for promoting the RISC rate. As a result, Th-BN exhibits not only a narrowband green emission at 512 nm, with a high luminous efficiency of 94% and a narrow FWHM of 41 nm/0.20 eV but also a rapid reverse intersystem crossing rate (k_{RISC} = 18.7 × 10^4 s^{-1}). Utilizing this excellent NB-MR-TADF molecule, the green OLEDs realized superior device performances, featuring a maximum external quantum efficiency (EQE_{max}) of up to 34.6% and high color purity with the coordinates of (0.23, 0.68). More importantly, a suppressed efficiency roll-off character with

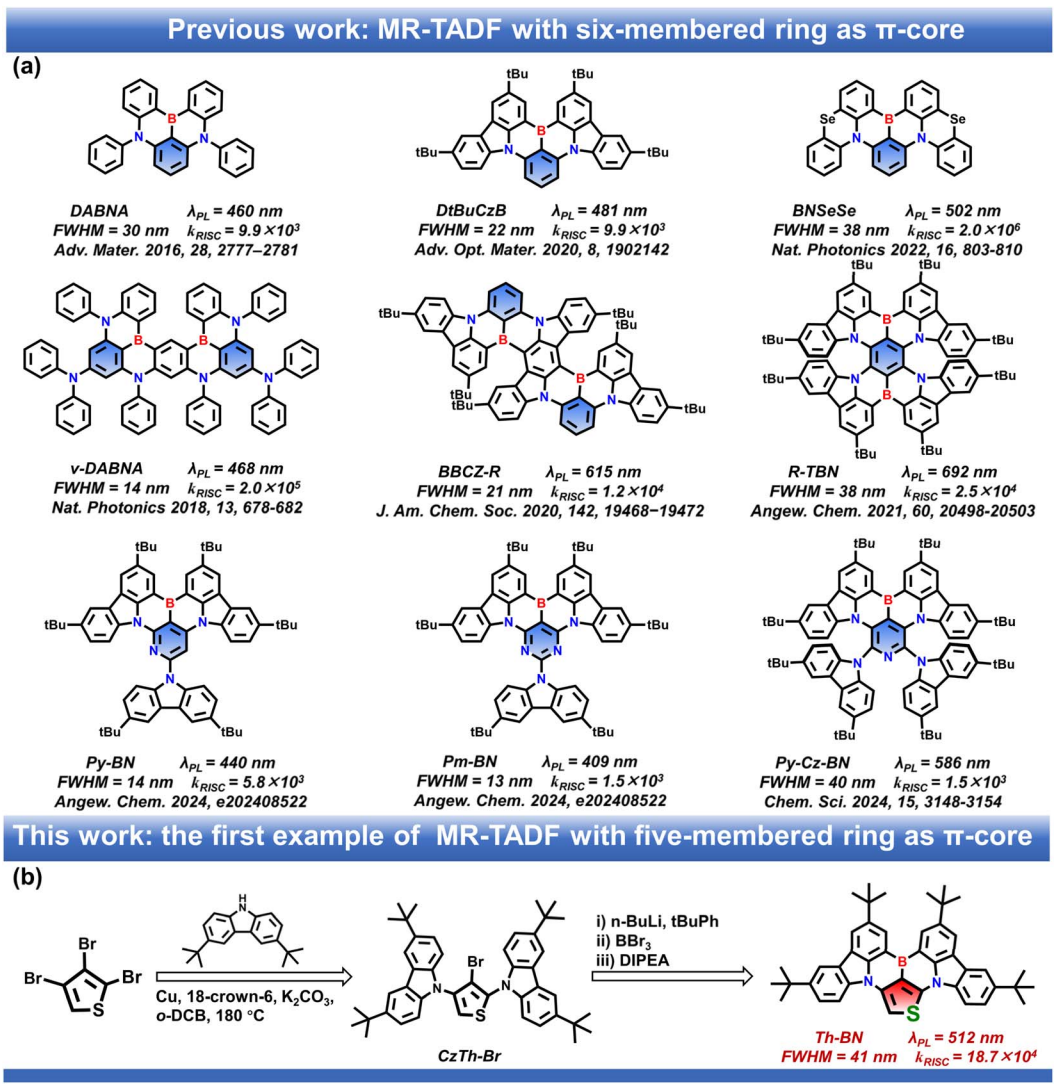

Fig. 1 Representatives of the reported MR-TADF emitters, molecular design strategy and synthetic routes of Th-BN.

an EQE of 26.8% at a high brightness of 1000 cd m^{-2} (corresponding to a low roll-off of 22.5%) was achieved. This work not only expands the diversity of MR molecular architectonics, but also opens up a new avenue to construct high-efficiency, high color purity and low efficiency roll-off OLEDs based on MR-TADF emitters with a five-membered ring π-core.

Results and discussion

The synthesis of Th-BN is illustrated in Fig. 1b. The intermediate CzTh-Br was prepared using the Buchwald–Hartwig coupling reaction from the commercially available starting materials of 3,6-di-*tert*-butyl-9*H*-carbazole and 2,3,4-tribromothiophene. The target molecule was obtained *via* a one-pot tandem lithiation–borylation–annulation reaction and purified by column chromatography as well as temperature-gradient sublimation. The chemical structure of Th-BN was fully characterized using nuclear magnetic resonance (NMR) spectra (Fig. S1 and S2, ESI†), mass spectra (Fig. S3 and S4, ESI†) and elemental analyses. The thermogravimetric analysis demonstrated that Th-BN had excellent thermal stability with a thermal decomposition temperature (T_d, corresponding to 5% weight-loss) of 427 °C (Fig. S5†) same as DtBuCzB. Based on cyclic voltammetry (CV) measurement, the LUMO energy level was estimated to be −2.54 eV for Th-BN (Fig. S6†). The HOMO energy level was estimated to be −4.99 eV from the optical bandgaps calculated from the onset of the UV-vis absorption spectrum of Th-BN (E_g = 2.45 eV, *vide infra*) and the LUMO energy level. Notably, Th-BN has a higher HOMO energy level and a smaller E_g compared to DtBuCzB, which explains the emission redshift.[54]

To deeply understand the impact of thiophene serving as the π-core in MR-TADF materials on the electronic structures, we first carried out density functional theory (DFT) calculations (Fig. S7†). The HOMO and LUMO distributions of Th-BN and DtBuCzB are very similar, showing alternative FMO density distributions. Consequently, the introduction of thiophene as the π-core in the MR-TADF emitter does not change the intrinsic MR properties. The calculated HOMO energy level of Th-BN is higher than that of DtBuCzB accompanied by identical

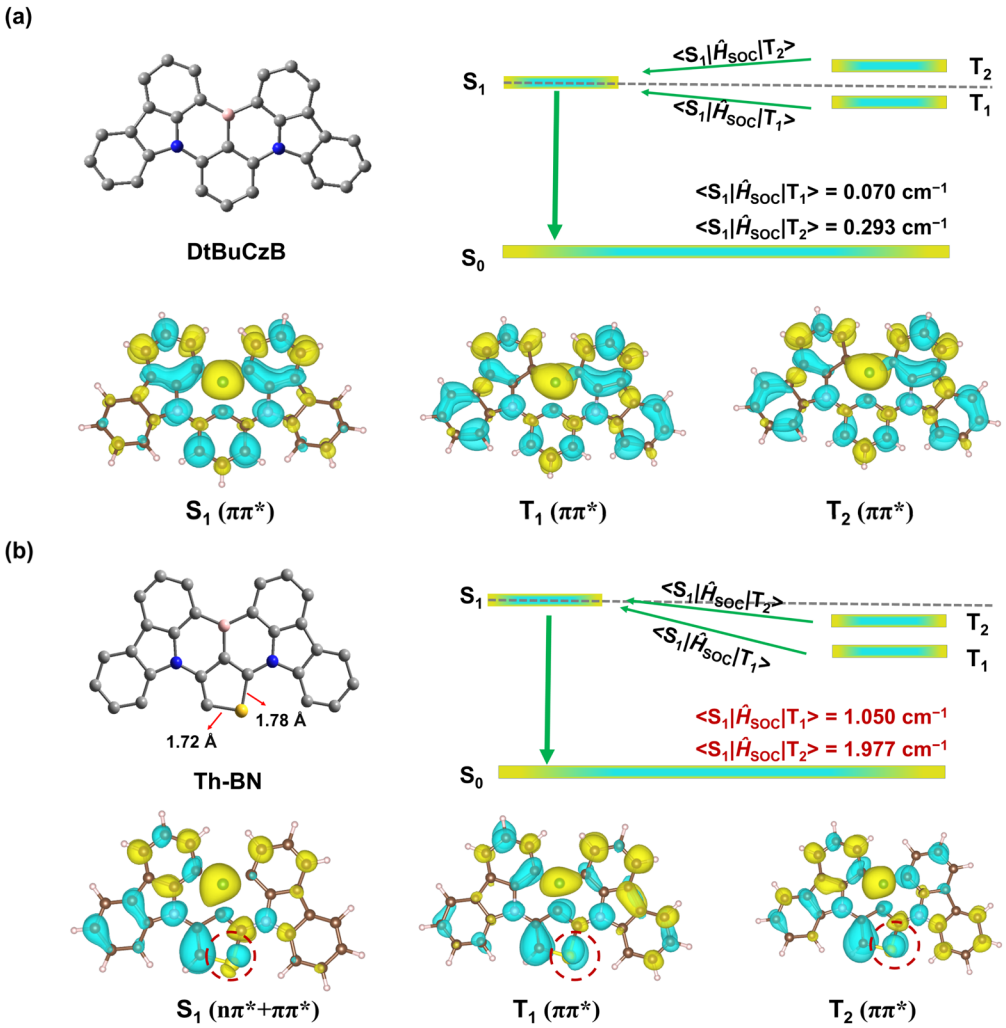

Fig. 2 Optimized geometries and calculated difference density plots of the S_1, T_1 and T_2 states at the STEOM-DLPNO-CCSD level of theory for DtBuCzB (a) and Th-BN (b).

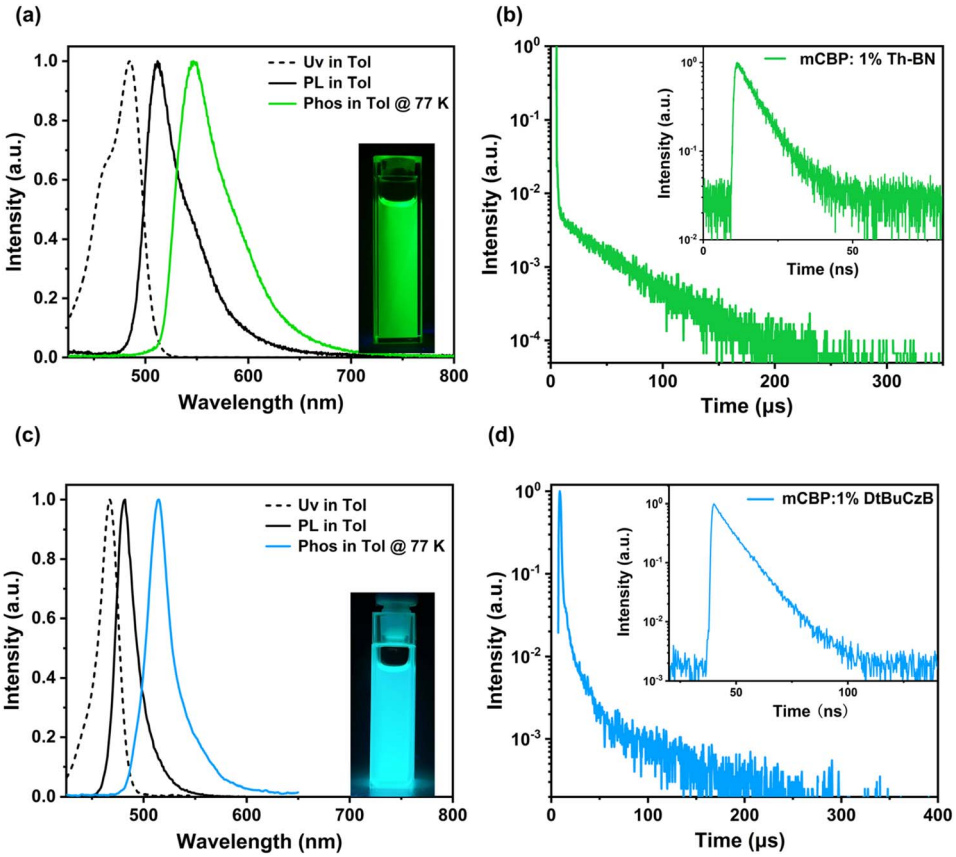

Fig. 3 (a) The normalized UV/vis absorption, fluorescence spectra (1×10^{-5} M, 298 K) and phosphorescence spectra (1×10^{-5} M, 77 K) of Th-BN measured in toluene solution. (b) Transient PL decay spectrum of the 1 wt% Th-BN: mCBP doped film. (c) The normalized UV/vis absorption, fluorescence spectra (1×10^{-5} M, 298 K) and phosphorescence spectra (1×10^{-5} M, 77 K) of DtBuCzB measured in toluene solution. (d) Transient PL decay spectrum of the 1 wt% DtBuCzB: mCBP doped film.

LUMO energy levels, resulting in a smaller HOMO–LUMO gap and an increased intramolecular charge transfer intensity of Th-BN. Additionally, due to the complex electronic configurations in the S_1 state, the orbital overlap integral β and charge transfer amount q are calculated between these orbitals (Table S1†). The smaller β and the larger q between these orbitals for Th-BN further confirm a significantly increased intramolecular charge transfer intensity for Th-BN. We also carried out high-level quantum-chemistry calculations on the excited states of DtBuCzB and Th-BN, *via* the STEOM-DLPNO-CCSD method adequately considering the electron-correlation effect. The relevant theoretical calculation details are given in the ESI.† Fig. 2 shows the difference density plots describing excitation characters of S_1, T_1 and T_2 states. Clearly, the orbitals of the

Table 1 Summary of the photophysical properties of DtBuCzB and Th-BN

	λ_{abs} [a] [nm]	λ_{PL} [b] [nm]	FWHM [c] [nm eV^{-1}]	E_{S_1} [d] [eV]	E_{T_1} [e] [eV]	ΔE_{ST} [f] [eV]	E_g [g] [eV]
DtBuCzB	467	481	22/0.11	2.73	2.58	0.15	2.55
Th-BN	485	512	41/0.20	2.55	2.41	0.14	2.45

	Φ_{PL} [h] [%]	τ_F [ns]	τ_{TADF} [μs]	k_{ISC} [10^7 s^{-1}]	k_{RISC} [10^4 s^{-1}]
DtBuCzB	90	8.5	68.8	2.3	1.8
Th-BN	97	7.0	40.7	12.4	18.7

[a] Peak wavelength of the lowest energy absorption band. [b] Peak wavelength of the PL spectrum in toluene (1×10^{-5} M, 298 K). [c] Full width at half maximum. [d] Singlet energy estimated from the onset of the fluorescence spectrum in toluene (1×10^{-5} M, 298 K). [e] Triplet energy estimated from the onset of the phosphorescence spectrum in a frozen toluene matrix (1×10^{-5} M, 77 K). [f] $\Delta E_{ST} = E_{S_1} - E_{T_1}$. [g] Optical band gap estimated from the absorption edge of the UV-vis spectrum. [h] Absolute photoluminescence quantum yield measured with an integrating sphere system in N_2-bubbling toluene.

electron-donating S atom contribute to the wavefunctions of the S_1, T_1 and T_2 states. Due to such a feature, the calculated S_1/T_1 excitation energy is 2.71/2.52 eV for Th-BN, lower than 2.81/2.62 eV for DtBuCzB. Their $\Delta E_{S_1T_1}$ values are thus almost the same, with 0.19 eV for Th-BN and DtBuCzB. The above calculation results are in line with our experimental ones, which confirms the reliability of our theoretical calculations. Moreover, our calculation results demonstrated that the energy gaps $\Delta E_{S_1T_2}$ between S_1 and T_2 states of DtBuCzB and Th-BN are small, *ca.* −0.06 and 0.03 eV, accompanied by $\Delta E_{T_2T_1}$ of 0.25 eV and 0.16 eV, respectively, which are small enough to facilitate the RISC process *via* the T_2-to-S_1 spin-flip channel. As shown in Fig. 2, for DtBuCzB, S_1, T_1 and T_2 states all show ππ* excitation character. Interestingly, for Th-BN, the S_1 state shows in addition to the dominant ππ* also a nπ* character, while its T_1 and T_2 are almost pure ππ* states. The difference in the excitation characters of S_1 and T_1/T_2 could arise from their different electronic configurations, see Fig. S8.† We found that the HOMO → LUMO/LUMO+1 configuration is overwhelmingly dominant in its T_1/T_2 states, while the electronic configurations are complex in its S_1 state, implying the importance of the electron-correlation effect. Usually, in thiophene or its derivatives, nπ* hardly contributes to the excited state due to its high excitation energy, since π-conjugation in the thiophene ring is strong and thus ππ* energy is low. However, compared to the C–S bond length of *ca.* 1.73 Å in a single thiophene ring, the optimized geometry of the π-core thiophene in Th-BN is largely deformed with a much longer C–S bond (*ca.* 1.78 Å), also see Fig. 2a. Such a longer C–S bond in Th-BN weakens intra-ring π-conjugation, which could make nπ* become feasible in the S_1 excitation. The SOC matrix elements of T_1–S_1 and T_2–S_1 transitions were further calculated (Table S2†). It is found that the SOC constants between S_1 and T_1/T_2 ($\langle S_1|\hat{H}_{SOC}|T_1/T_2\rangle$) are just 0.07/0.29 cm^{-1} for DtBuCzB. In contrast, for Th-BN, due to the difference between the excitation characters of S_1 and T_1/T_2, $\langle S_1|\hat{H}_{SOC}|T_1/T_2\rangle$ is much larger, *ca.* 1.05/1.98 cm^{-1}. Finally, a rapid RISC process from T_1 and T_2 to the S_1 channel occurs in Th-BN; the calculated Boltzmann-average k_{RISC} for Th-BN is 57.6 × 10^4 s^{-1}, much faster than that of DtBuCzB (0.73 × 10^4 s^{-1}) (Table S3†). Our theoretical results support our molecular design, suggesting that the introduction of the thiophene π-core can significantly improve the SOC due to different excitation characters between singlet and triplet states, and thus accelerate the RISC process.

Th-BN in dilute toluene solution (concentration: 10^{-5} M) is depicted in Fig. 3 and the detailed photophysical data are summarized in Table 1. Compared with DtBuCzB which exhibits a maximum absorption band at 467 nm, Th-BN presents an obviously red-shifted absorption peak at 506 nm, which is ascribed to the HOMO–LUMO transition characterized by MR-induced short-range charge-transfer. The optical band gap of Th-BN is calculated to be 2.40 eV based on the onset wavelength of the absorption spectrum. In the fluorescence spectrum, Th-BN exhibits a mirror image and bright green emission with a dominant peak at 512 nm and a high photoluminescence quantum yield (Φ_{PL}) of 97%. The maximum emission wavelength of Th-BN is red-shifted by 31 nm compared to that of DtBuCzB, attributed to increased intramolecular charge transfer intensity from the introduction of the thiophene π-core. A small Stokes shift value of 6 nm evidences a small vibronic coupling between the ground state and excited state as well as the small structural relaxation in the S_1 state, which leads to a narrow FWHM of 41 nm/0.20 eV. Additionally, as the polarity of the solvent increases from nonpolar cyclohexane to highly polar dichloromethane, Th-BN exhibits stronger positive solvatochromism and solvent-dependent spectral profile characteristics compared to DtBuCzB, indicating the increased intramolecular charge-transfer properties of Th-BN (Fig. S9 and Table S4†). From the onsets of the fluorescence spectrum at 298 K and the phosphorescence spectrum recorded in frozen toluene at 77 K, the S_1/T_1 energy levels (E_{S_1}/E_{T_1}) were estimated to be 2.55/2.41 eV for Th-BN. Therefore, a small ΔE_{ST} value is calculated to be 0.14 eV, which is slightly lower than that of DtBuCzB (0.15 eV), benefiting the RISC process from the T_1 state to the S_1 state.[55–58]

The photophysical properties of Th-BN were further investigated by dispersing it in a wide energy-gap host, 3,3′-di(carbazol-9-yl)biphenyl (mCBP), with a doping concentration of 1 wt%. As shown in Fig. S10, ESI,† the doped film of Th-BN exhibited a narrowband green emission with a peak wavelength at 512 nm and a FWHM of 48 nm, which is very similar to the result in toluene. The slight spectral broadening in the doped film is associated with the possible host–guest interactions, which are common for MR-TADF emitters due to their rigid planar molecular structures.[59–61] At room temperature and in a vacuum atmosphere, Th-BN shows a short-lived prompt lifetime (τ_F) of 7.0 ns and a long-lived delay lifetime (τ_{TADF}) of 40.7 μs with the percentage of delayed component of 86.4% (Table S5, ESI†). The TADF nature of Th-BN was further confirmed by temperature-dependent transient PL decay measurements (Fig. S11, ESI†). As the temperature increases from 200 to 300 K, the proportion of delayed fluorescence components increases gradually, further confirming the TADF characteristics of Th-BN. Moreover, a high PLQY of 94% was obtained, evidencing the efficient radiative decay process. Benefiting from the high SOC value of Th-BN, the estimated rate constant of the reverse intersystem crossing (k_{RISC}) is as high as 18.7 × 10^4 s^{-1} and 10 times higher than that of its analogue DtBuCzB (1.8 × 10^4 s^{-1}),[62–65] evidencing the effectiveness of our proposed design strategy. To the best of our knowledge, the obtained k_{RISC} value far surpasses those of most reported MR-TADF emitters and is comparable to the level of a classic MR-TADF emitter *ν*-DABNA (2.0 × 10^5 s^{-1}).[66] The above photophysical data summarized in Table 1 demonstrate that Th-BN is a promising MR-TADF emitter for high-efficiency, high color purity and low efficiency roll-off OLEDs.

Inspired by the excellent photoluminescent properties of Th-BN, vacuum-deposited OLEDs were evaluated with the following device configuration: indium tin oxide (ITO)/1,1-bis[(di-4-tolylamino)phenyl]cyclohexane (TAPC, 50 nm)/tris(4-carbazolyl-9-ylphenyl)amine (TCTA, 5 nm)/*x* wt% Th-BN in 5-(4-(4,6-diphenyl-1,3,5-triazin-2-yl)phenyl)-7,7-dimethyl-5,7-dihydroindeno[2,1-*b*]carbazole (InCz23DMeTz 30 nm)/(3,3'-[5'-[3-(3-Pyridinyl)phenyl][1,1′:3′,1″-terphenyl]-3,3″-diyl]bispyridine)

Table 2 Summary of the electroluminescence data of the Th-BN and DtBuCzB-based devices

Device	x wt [%]	λ_{EL}[a] [nm]	FWHM[b] [nm]	V_{on}[c] [V]	L_{max}[d] [cd m^{-2}]	CE_{max}[e] [cd A^{-1}]	PE_{max}[f] [lm W^{-1}]	EQE[g] [%]	CIE (x, y)[h]
A	1.0	516	41	2.7	60 440	122.9	134.3	34.6/34.0/26.8	(0.23, 0.68)
B	2.0	520	42	2.6	62 050	112.9	125.2	32.6/31.6/26.2	(0.25, 0.68)
C	3.0	524	45	2.6	60 170	95.7	105.7	26.9/26.6/22.9	(0.27, 0.67)
D	1.0	490	28	3.3	17 150	40.2	35.1	21.9/11.1/6.9	(0.09, 0.36)

[a] EL maximum wavelength. [b] Full width at half maximum. [c] Turn-on voltage at 1 cd m^{-2}. [d] Maximum luminance. [e] Maximum current efficiency. [f] Maximum power efficiency. [g] Maximum external quantum efficiency and values at 100 and 1000 cd m^{-2}. [h] Value at 100 cd m^{-2}.

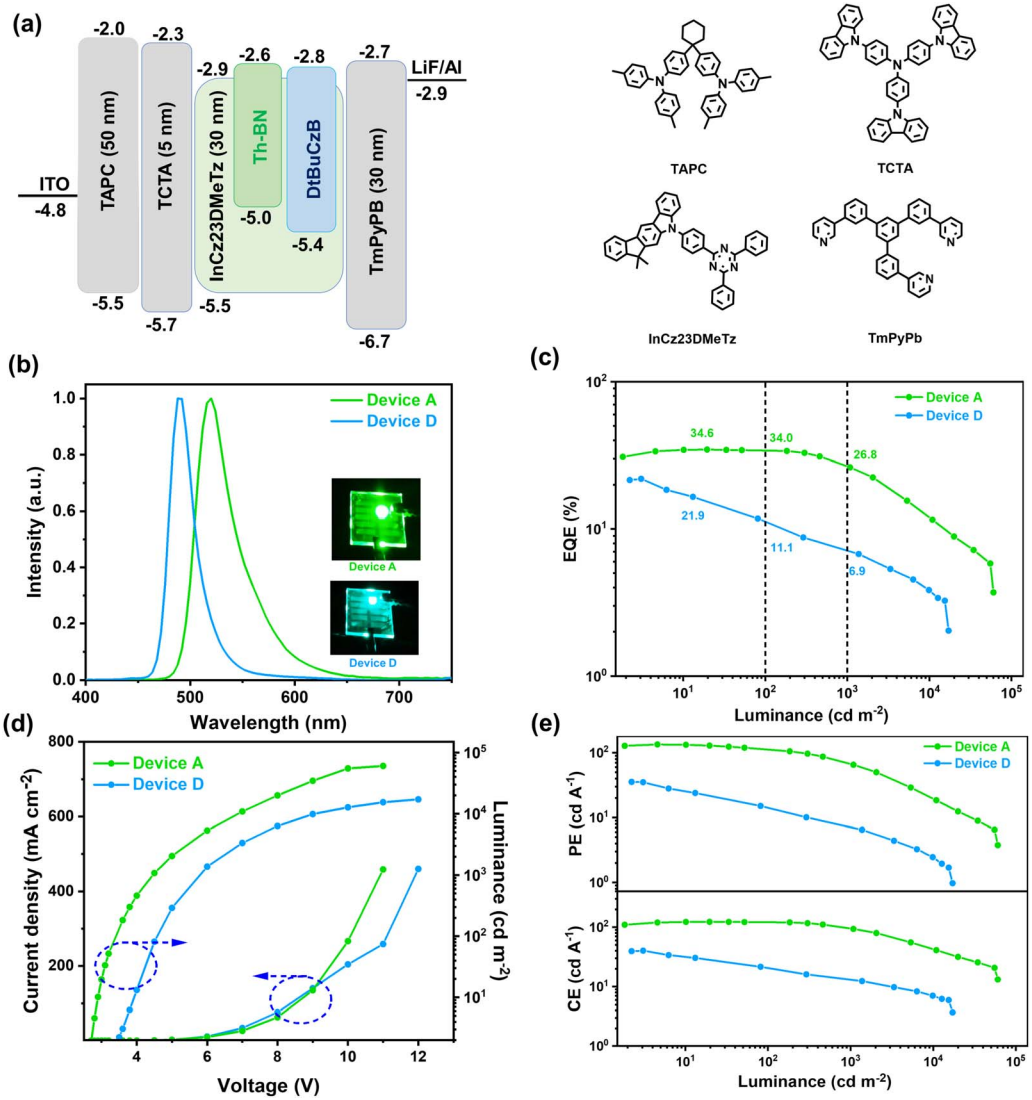

Fig. 4 OLED performances of the doped devices. (a) Device structure with the energy-level diagrams. (b) EL curves. (c) EQE–L curves. (d) J–V–L curves. (e) CE–L and PE–L curves.

(TmPyPB, 30 nm)/lithium fluoride (LiF, 1 nm)/aluminum (Al, 100 nm) (x = 1, 2 and 3 for devices A–C). All device data are summarized in Table 2 and selectively presented in Fig. 4. The corresponding energy level diagrams of the devices and the molecular structures of the used materials used are illustrated in Fig. 4a. In these devices, ITO and Al served as the anode and cathode, respectively; TAPC and TCTA, TmPyPB and LiF functioned as the hole-transporting layer, the electron-blocking, the electron-transporting layer and the electron-injection layer, respectively. And the device D using DtBuCzB with 1 wt% doping concentration as the emitter was also fabricated for comparison (Table 2).

All devices have low turn-on voltages (V_{on}) of below 2.7 V (recorded at a brightness of 1 cd m^{-2}), attributed to the suitable energy level cascade between the emitting layer and the functional layers. Devices A–C all exhibit narrowband green emissions with EL peaks from 516 to 524 nm and FWHM values from 41 to 45 nm. The corresponding Commission Internationale de l'Eclairage (CIE) coordinates are (0.23, 0.68), (0.25, 0.68) and (0.27, 0.67), respectively (Fig. S12†). With the increase of doping concentration from 1 to 3 wt%, the EL spectra display slight red-shift and broadening, which is consistent with PL spectra of the doped films. Furthermore, devices A–C exhibit excellent EL performance, including high maximum external quantum efficiencies (EQEs) of 34.6–26.9%, current efficiencies (CEs) of 122.9–95.7 cd A^{-1} and power efficiencies (PEs) of 134.3–105.7 lm W^{-1} (Fig. S12†). Among them, device A with 1 wt% doping concentration gives the optimal device performance with maximum EQE, CE and PE of 34.6%, 122.9 cd A^{-1} and 134.3 lm W^{-1}, respectively (Fig. 4). It is worth noting that at a practical application luminance of 1000 cd m^{-2}, the EQE value of device B still maintains as high as 26.8%, corresponding to a low roll-off of 22.5%. In contrast, device D demonstrates a maximum external quantum efficiency of 21.9% and a serious efficiency roll-off with an EQE value of 6.9% at 1000 cd m^{-2} owing to the slow k_{RISC} rate (Fig. 4). The low efficiency roll-off characteristic of Th-BN-based devices is ascribed to its efficient upconversion of triplet excitons to suppress the triplet-involved annihilation processes in the devices.

Conclusions

In conclusion, we have developed for the first time a novel MR-TADF emitter based on a five-membered ring π-core and achieved superior EL performance compared to the benzenoid π-core-based analogue. A proof-of-concept molecule Th-BN with a thiophene π-core was developed, exhibiting a narrowband green emission at 512 nm with a FWHM of 41 nm and a high Φ_{PL} of 97% in toluene solution. Moreover, owing to the heavy-atom effect of the S atom and increased nπ* character of the S_1 state, a rapid RISC rate of 18.7×10^4 s^{-1} is achieved. Devices based on Th-BN display excellent EL performances, including maximum EQE, CE and PE of 34.6%, 122.9 cd A^{-1} and 134.3 lm W^{-1}, respectively. More importantly, a low efficiency roll-off with an EQE of 26.8% at a high brightness of 1000 cd m^{-2} was achieved. Our results highlight the five-membered thiophene π-core as a promising alternative building block in the molecular design of MR-TADF emitters for highly efficient OLEDs with narrowband emission, high color purity and low efficiency roll-off.

Data availability

All data supporting this study are available in the article and ESI.†

Author contributions

L. L. carried out most parts of the experiments and wrote the original manuscript. J. L. and X.-K. C. were responsible for theoretical calculations. L. G., Y. X. and P. Z. analyzed the data and provided comments. Y. P. and Y. B. fabricated OLED devices. C. L. and Y. W. supervised the project, analyzed the data and revised the manuscript. The authors would thank Miss Wei Xin for designing the artwork in this article.

Conflicts of interest

There are no conflicts to declare.

Acknowledgements

This work was supported by the National Natural Science Foundation of China (52173165), the National Key R&D Program of China (2020YFA0714601), the Natural Science Foundation of Chongqing, China (cstc2021jcyj-msxmX0274), Open Fund of the Key Lab of Organic Optoelectronics and Molecular Engineering of Ministry of Education (53223000122), and the Science, Technology Research Project of the Education Department of Jilin Province, China (JJKH20241245KJ).

References

1 G. Hong, X. Gan, C. Leonhardt, Z. Zhang, J. Seibert, J. M. Busch and S. Bräse, *Adv. Mater.*, 2021, **33**, 2005630.
2 Y. Liu, C. Li, Z. Ren, S. Yan and M. R. Bryce, *Nat. Rev. Mater.*, 2018, **3**, 18020.
3 C. W. Tang and S. A. VanSlyke, *Appl. Phys.*, 1978, **51**, 913–915.
4 L.-S. Cui, A. J. Gillett, S.-F. Zhang, H. Ye, Y. Liu, X.-K. Chen, Z.-S. Lin, E. W. Evans, W. K. Myers, T. K. Ronson, H. Nakanotani, S. Reineke, J.-L. Bredas, C. Adachi and R. H. Friend, *Nat. Photonics*, 2021, **15**, 203–207.
5 H. Uoyama, K. Goushi, K. Shizu, H. Nomura and C. Adachi, *Nature*, 2021, **492**, 234–238.
6 I. S. Park, K. Matsuo, N. Aizawa and T. Yasuda, *Adv. Funct. Mater.*, 2018, **28**, 1802031.
7 S. MadayanadSuresh, D. Hall, D. Beljonne, Y. Olivier and E. Zysman-Colman, *Adv. Funct. Mater.*, 2020, **30**, 1908677.
8 J. S. Steckel, P. Snee, S. Coe-Sullivan, J. P. Zimmer, J. E. Halpert, P. Anikeeva, L.-A. Kim, V. Bulovic and M. G. Bawendi, *Angew. Chem., Int. Ed.*, 2006, **45**, 5796–5799.
9 T. Hatakeyama, K. Shiren, K. Nakajima, S. Nomura, S. Nakatsuka, K. Kinoshita, J. Ni, Y. Ono and T. Ikuta, *Adv. Mater.*, 2016, **28**, 2777–2781.
10 Y. Kondo, K. Yoshiura, S. Kitera, H. Nishi, S. Oda, H. Gotoh, Y. Sasada, M. Yanai and T. Hatakeyama, *Nat. Photonics*, 2019, **13**, 678–682.
11 S. Oda, T. Sugitani, H. Tanaka, K. Tabata, R. Kawasumi and T. Hatakeyama, *Adv. Mater.*, 2022, **34**, 2201778.
12 S. Cai, G. S. M. Tong, L. Du, G. K.-M. So, F.-F. Hung, T.-L. Lam, G. Cheng, H. Xiao, X. Chang, Z.-X. Xu and C.-M. Che, *Angew. Chem., Int. Ed.*, 2022, **61**, e202213392.
13 J. Bian, S. Chen, L. Qiu, R. Tian, Y. Man, Y. Wang, S. Chen, J. Zhang, C. Duan, C. Han and H. Xu, *Adv. Mater.*, 2022, **34**, 2110547.

14 Y.-C. Cheng, X.-C. Fan, F. Huang, X. Xiong, J. Yu, K. Wang, C.-S. Lee and X.-H. Zhang, *Angew. Chem., Int. Ed.*, 2022, **61**, e202212575.
15 H. J. Kim and T. Yasuda, *Adv. Opt. Mater.*, 2022, **10**, 2201714.
16 Y. Zhang, J. Wei, D. Zhang, C. Yin, G. Li, Z. Liu, X. Jia, J. Qiao and L. Duan, *Angew. Chem., Int. Ed.*, 2022, **61**, e202113206.
17 X.-C. Fan, K. Wang, Y.-Z. Shi, Y.-C. Cheng, Y.-T. Lee, J. Yu, X.-K. Chen, C. Adachi and X.-H. Zhang, *Nat. Photonics*, 2023, **17**, 280–285.
18 X.-L. Chen, J.-H. Jia, R. Yu, J.-Z. Liao, M.-X. Yang and C.-Z. Lu, *Angew. Chem., Int. Ed.*, 2017, **56**, 15006–15009.
19 S. H. Han, J. H. Jeong, J. W. Yoo and J. Y. Lee, *J. Mater. Chem. C*, 2019, **7**, 3082–3089.
20 X. Liang, Z.-P. Yan, H.-B. Han, Z.-G. Wu, Y.-X. Zheng, H. Meng, J.-L. Zuo and W. Huang, *Angew. Chem., Int. Ed.*, 2018, **57**, 11316–11320.
21 S. Oda, W. Kumano, T. Hama, R. Kawasumi, K. Yoshiura and T. Hatakeyama, *Angew. Chem., Int. Ed.*, 2021, **60**, 2882–2886.
22 J. A. Knöller, G. Meng, X. Wang, D. Hall, A. Pershin, D. Beljonne, Y. Olivier, S. Laschat, E. Zysman-Colman and S. Wang, *Angew. Chem., Int. Ed.*, 2020, **59**, 3156–3160.
23 M. Yang, S. Shikita, H. Min, I. S. Park, H. Shibata, N. Amanokura and T. Yasuda, *Angew. Chem., Int. Ed.*, 2021, **60**, 23142–23147.
24 K. Matsui, S. Oda, K. Yoshiura, K. Nakajima, N. Yasuda and T. Hatakeyama, *J. Am. Chem. Soc.*, 2018, **140**, 1195–1198.
25 J. Park, J. Lim, J. H. Lee, B. Jang, J. H. Han, S. S. Yoon and J. Y. Lee, *ACS Appl. Mater. Interfaces*, 2021, **13**, 45798–45805.
26 P. Jiang, L. Zhan, X. Cao, X. Lv, S. Gong, Z. Chen, C. Zhou, Z. Huang, F. Ni, Y. Zou and C. Yang, *Adv. Opt. Mater.*, 2021, **9**, 2100825.
27 Y. Zhang, D. Zhang, J. Wei, X. Hong, Y. Lu, D. Hu, G. Li, Z. Liu, Y. Chen and L. Duan, *Angew. Chem., Int. Ed.*, 2020, **59**, 17499–17503.
28 J. Liu, Y. Zhu, T. Tsuboi, C. Deng, W. Lou, D. Wang, T. Liu and Q. Zhang, *Nat. Commun.*, 2022, **13**, 4876.
29 J.-J. Hu, X.-F. Luo, Y.-P. Zhang, M.-X. Mao, H.-X. Ni, X. Liang and Y.-X. Zheng, *J. Mater. Chem. C*, 2022, **10**, 768–773.
30 G. Liu, H. Sasabe, K. Kumada, A. Matsunaga, H. Katagiri and J. Kido, *J. Mater. Chem. C*, 2021, **9**, 8308–8313.
31 F. Liu, Z. Cheng, Y. Jiang, L. Gao, H. Liu, H. Liu, Z. Feng, P. Lu and W. Yang, *Angew. Chem., Int. Ed.*, 2022, **61**, e202116927.
32 M. Yang, I. S. Park and T. Yasuda, *J. Am. Chem. Soc.*, 2020, **142**, 19468–19472.
33 Y. Zhang, D. Zhang, T. Huang, A. J. Gillett, Y. Liu, D. Hu, L. Cui, Z. Bin, G. Li, J. Wei and L. Duan, *Angew. Chem., Int. Ed.*, 2021, **60**, 20498–20503.
34 Y. Zou, J. Hu, M. Yu, J. Miao, Z. Xie, Y. Qiu, X. Cao and C. Yang, *Adv. Mater.*, 2022, **34**, 2201442.
35 X. Cai, Y. Xu, Y. Pan, L. Li, Y. Pu, X. Zhuang, C. Li and Y. Wang, *Angew. Chem., Int. Ed.*, 2023, **62**, e202216473.
36 J.-K. Li, X.-Y. Chen, Y.-L. Guo, X.-C. Wang, A. C. H. Sue, X.-Y. Cao and X.-Y. Wang, *J. Am. Chem. Soc.*, 2021, **143**, 17958–17963.
37 T. Fan, M. Du, X. Jia, L. Wang, Z. Yin, Y. Shu, Y. Zhang, J. Wei, D. Zhang and L. Duan, *Adv. Mater.*, 2023, **35**, 2301018.
38 X.-C. Fan, K. Wang, Y.-Z. Shi, J.-X. Chen, F. Huang, H. Wang, Y.-N. Hu, Y. Tsuchiya, X.-M. Ou, J. Yu, C. Adachi and X.-H. Zhang, *Adv. Opt. Mater.*, 2022, **10**, 2101789.
39 X. Cai, Y. Pan, C. Li, L. Li, Y. Pu, W. W and Y. Wang, *Angew. Chem., Int. Ed.*, 2024, e202408522.
40 M. Du, M. Mai, D. Zhang, L. Duan and Y. Zhang, *Chem. Sci.*, 2024, **15**, 3148–3154.
41 C. Duan, K. Gao, F. J. M. Colberts, F. Liu, S. C. J. Meskers, M. M. Wienk and R. A. J. Janssen, *Adv. Energy Mater.*, 2017, **7**, 1700519.
42 J. J. Dressler, M. Teraoka, G. L. Espejo, R. Kishi, S. Takamuku, C. J. Gómez-García, L. N. Zakharov, M. Nakano, J. Casado and M. M. Haley, *Chem. Soc. Nature Chem. Rev.*, 2018, **10**, 1134–1140.
43 C. W. Zhuang, M. Bolognesi, M. Seri, P. Henriksson, D. Gedefaw, R. Kroon, M. Jarvid, A. Lundin, E. Wang, M. Muccini and M. R. Andersson, *Macromolecules*, 2013, **46**, 8488–8499.
44 Y. Chen, Y. Zheng, Y. Jiang, H. Fan and X. Zhu, *J. Am. Chem. Soc.*, 2021, **143**, 4281–4289.
45 R. Qin, W. Li, C. Li, C. Du, C. Veit, H.-F. Schleiermacher, M. Andersson, Z. Bo, Z. Liu, O. Inganäs, U. Wuerfel and F. Zhang, *J. Am. Chem. Soc.*, 2009, **131**, 14612–14613.
46 H. Maruo, Y. Sasaki, K. Harada, K. Suwa, K. Oyaizu, H. Segawa, K. Carter and H. Nishide, *Polym. J.*, 2019, **51**, 91–96.
47 D. C. Kim, H. J. Shim, W. Lee, J. H. Koo and D.-H. Kim, *Adv. Mater.*, 2020, **32**, 1902743.
48 M. Saito, I. Osaka, Y. Suzuki, K. Takimiya, T. Okabe, S. Ikeda and T. Asano, *Sci. Rep.*, 2015, **5**, 14202.
49 X. Han, Y. Zhang, Y. Dong, J. Zhao, S. Ming and J. Zhang, *RSC Adv.*, 2022, **12**, 708–718.
50 X. Yuan, K. Yang, C. Grazon, C. Wang, L. Vallan, J.-D. Isasa, P. M. Resende, F. Li, C. Brochon, H. Remita, G. Hadziioannou, E. Cloutet and J. Li, *Angew. Chem., Int. Ed.*, 2024, **63**, e202315333.
51 T. Banerjee, F. Podjaski, J. Kröger, B. P. Biswal and B. V. Lotsch, *Nat. Rev. Mater.*, 2021, **6**, 168–190.
52 C. Yang, S. Zhang and J. Hou, *Aggregate*, 2022, **3**, e111.
53 Y. Xu, Z. Cheng, Z. Li, B. Liang, J. Wang, J. Wei, Z. Zhang and Y. Wang, *Adv. Opt. Mater.*, 2020, **8**, 1902142.
54 Y. Zhang, D. Zhang, J. Wei, Z. Liu, Y. Lu and L. Duan, *Angew. Chem., Int. Ed.*, 2019, **58**, 16912–16917.
55 Y. Hu, J. Miao, T. Hua, Z. Huang, Y. Qi, Y. Zou, Y. Qiu, H. Xia, H. Liu, X. Cao and C. Yang, *Nat. Photonics*, 2022, **16**, 803–810.
56 Y. Hu, J. Miao, C. Zhong, Y. Zeng, S. Gong, X. Cao, X. Zhou, Y. Gu and C. Yang, *Angew. Chem., Int. Ed.*, 2023, **62**, e202302478.
57 I. S. Park, H. Min and T. Yasuda, *Angew. Chem., Int. Ed.*, 2022, **61**, e202205684.
58 M. Nagata, H. Min, E. Watanabe, H. Fukumoto, Y. Mizuhata, N. Tokitoh, T. Agou and T. Yasuda, *Angew. Chem., Int. Ed.*, 2021, **60**, 20280.
59 Y. Liu, X. Xiao, Z. Huang, D. Yang, D. Ma, J. Liu, B. Lei, Z. Bin and J. You, *Angew. Chem., Int. Ed.*, 2022, **61**, e202210210.
60 Q. Wang, Y. Xu, T. Yang, J. Xue and Y. Wang, *Adv. Mater.*, 2023, **35**, 2205166.

61 J. Jin, C. Duan, H. Jiang, P. Tao, H. Xu and W.-Y. Wong, *Angew. Chem., Int. Ed.*, 2023, **62**, e202218947.
62 X.-F. Luo, S.-Q. Song, H.-X. Ni, H. Ma, D. Yang, D. Ma, Y.-X. Zheng and J.-L. Zuo, *Angew. Chem., Int. Ed.*, 2022, **61**, e202209984.
63 X.-F. Luo, H.-X. Ni, A.-Q. Lv, X.-K. Yao, H.-L. Ma and Y.-X. Zheng, *Adv. Opt. Mater.*, 2022, **10**, 2200504.
64 Q. Zhang, S. Sun, W. Liu, P. Leng, X. Lv, Y. Wang, H. Chen, S. Ye, S. Zhuang and L. Wang, *J. Mater. Chem. C*, 2019, **7**, 9487–9495.
65 K. R. Naveen, H. I. Yang and J. H. Kwon, *Commun. Chem.*, 2022, **5**, 149.
66 P. K. Samanta, D. Kim, V. Coropceanu and J.-L. Brédas, *J. Am. Chem. Soc.*, 2017, **139**, 4042–4051.